Herbivore feeding preference corroborates optimal defense theory for specialized metabolites within plants

Pascal Hunziker[a,1], Sophie Konstanze Lambertz[a], Konrad Weber[a], Christoph Crocoll[a], Barbara Ann Halkier[a,2], and Alexander Schulz[a,2]

[a]DynaMo Center, Department of Plant and Environmental Sciences, University of Copenhagen, 1871 Frederiksberg C, Denmark

Edited by Richard A. Dixon, University of North Texas, Denton, TX, and approved October 19, 2021 (received for review June 29, 2021)

Numerous plants protect themselves from attackers by using specialized metabolites. The biosynthesis of these deterrent, often toxic metabolites is costly, as their synthesis diverts energy and resources on account of growth and development. How plants diversify investments into growth and defense is explained by the optimal defense theory. The central prediction of the optimal defense theory is that plants maximize growth and defense by concentrating specialized metabolites in tissues that are decisive for fitness. To date, supporting physiological evidence relies on the correlation between plant metabolite presence and animal feeding preference. Here, we use glucosinolates as a model to examine the effect of changes in chemical defense distribution on feeding preference. Taking advantage of the uniform glucosinolate distribution in transporter mutants, we show that high glucosinolate accumulation in tissues important to fitness protects them by guiding larvae of a generalist herbivore to feed on other tissues. Moreover, we show that the mature leaves of *Arabidopsis thaliana* supply young leaves with glucosinolates to optimize defense against herbivores. Our study provides physiological evidence for the central hypothesis of the optimal defense theory and sheds light on the importance of integrating glucosinolate biosynthesis and transport for optimizing plant defense.

metabolite transport | glucosinolate | defense | herbivore | optimal defense theory

Spatial and temporal variation of metabolically costly defenses within a plant is rationalized by the optimal defense theory, which predicts that defenses have evolved and are allocated based on the fitness value and vulnerability of individual plant parts to simultaneously optimize growth and defense (1–3). Much research in plant defense theory is focused on its ecological–evolutionary facets—studying whether organisms evolve defenses proportional to their risk of being attacked and inversely proportional to the cost of defense—which addresses one important aspect of the optimal defense theory (4, 5). A significant number of physiological investigations into optimal defense within individual plants reported correlation between defense distribution and either herbivore feeding preference, risk of attack, or plant fitness (4, 6). Moving beyond correlational tests of predictions of the optimal defense theory for within-plant defense distribution, plants genetically modified to eliminate biosynthesis or activation of defensive metabolites were exploited to indicate a causal link between defensive metabolites and herbivore feeding preference (7–9). Although these findings reveal the benefit of defense for the plant, they are based on comparing mutant plants without such metabolites with wild-type (WT) plants in which the defense is not uniformly distributed. Because of the lack of genetic tools to manipulate chemical defense distribution without eliminating them, empirical studies addressing the effect of optimal defense distribution within a plant on animal feeding preference and behavior are still missing. Here, we asked how the allocation of chemical defense compounds affects herbivore feeding preference using glucosinolates in *Arabidopsis thaliana* as a model.

Glucosinolates are amino acid–derived thioglucosides that yield herbivore-deterrent catabolites upon tissue damage–triggered enzymatic hydrolysis by myrosinases (10). However, many herbivores circumvent glucosinolate-based defenses via diverse behavioral and physiological counteradaptations (11). High selective pressure by coevolving predators conserved the production of glucosinolates despite large energy costs (12, 13). *A. thaliana* meets the predictions of the optimal defense theory: Young leaves are more valuable than old ones and display much higher glucosinolate concentration (14, 15). Similar ontogenetic patterns were reported for many other species of the Brassicales order, indicating existence of a universal glucosinolate distribution pattern (16–20). To examine the glucosinolate distribution in rosettes of the reference plant *A. thaliana*, we grouped leaves of 5-wk-old plants into three cohorts according to their age (Fig. 1*A*). Liquid chromatography–mass spectrometry (LC-MS) revealed that the total glucosinolate concentration is highest in young leaves and decreases gradually with leaf age (Fig. 1*B*). To investigate whether the ontogenetic pattern of glucosinolate concentrations across the rosette correlate with transcript levels of key enzymes involved in glucosinolate biosynthesis, we measured the expression of *CYP79B2*, *CYP83A1*, *MAM1*, *MAM3*,

Significance

The "optimal defense theory" is a long-standing theoretical framework that is still controversially discussed. The central hypothesis of the optimal defense theory predicts that plant defenses are concentrated at the highest level in tissues and in organs that are the most valuable for survival and fitness. In this paper, we use the herbivore-deterrent defense compounds glucosinolates in the reference plant *Arabidopsis thaliana* as a model to test this central aspect of the optimal defense theory. We eliminated the gradient of glucosinolate distribution across tissues by the mutation of genes encoding transporters and thereby altered the feeding preference of the African cotton leafworm, *Spodoptera littoralis*, which is a devastating pest of many economically important crop plants including cotton, tomato, and maize.

Author contributions: P.H., S.K.L., B.A.H., and A.S. designed research; P.H., S.K.L., K.W., and C.C. performed research; P.H., S.K.L., K.W., and C.C. analyzed data; B.A.H. and A.S. provided supervision; and P.H., B.A.H., and A.S. wrote the paper.

The authors declare no competing interest.

This article is a PNAS Direct Submission.

See online for related content such as Commentaries.

[1]Present address: Centre for Organismal Studies, Heidelberg University, 69120 Heidelberg, Germany.

[2]To whom correspondence may be addressed. Email: bah@plen.ku.dk or als@plen.ku.dk.

This article contains supporting information online at http://www.pnas.org/lookup/suppl/doi:10.1073/pnas.2111977118/-/DCSupplemental.

Published November 18, 2021.

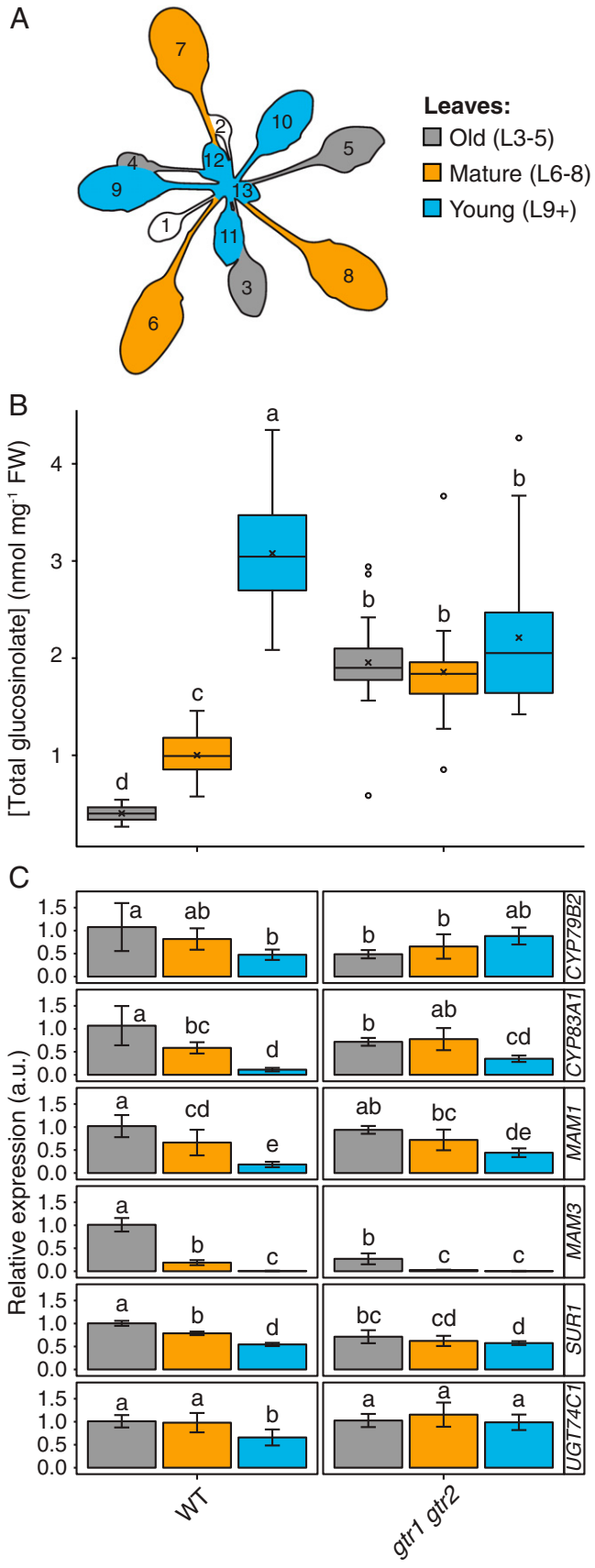

Fig. 1. Tissue-specific analysis of glucosinolate concentrations and biosynthetic gene expression in transporter knockout mutants. (*A*) Harvesting scheme depicting the silhouette of an *A. thaliana* rosette used for sampling. Leaves are numbered according to ontogenetic development starting with the first true leaf. Colors indicate the grouping into cohorts of old (L3-5; gray), mature (L6-8; orange), and young leaves (L9+; blue). (*B*) Tissue-specific total glucosinolate concentration of WT and *gtr1 gtr2* double transporter knockout mutants. Colors indicate leaf cohorts according to *A*. Letters indicate significant differences of genotype × tissue interactions (two-way ANOVA with post hoc Tukey's HSD test; $n = 10$; $P < 0.001$). Pooled data from two independent replicates are shown. "x" indicates mean. FW, fresh weight.(*C*) Expression analysis of glucosinolate biosynthetic genes in WT and *gtr1gtr2* mutants. Colors indicate leaf cohorts according to *A*. Transcript levels of *CYP79B2*, *CYP83A1*, *MAM1*, *MAM3*, *SUR1*, and *UGT74C1* are shown relative to the abundance in old leaves (L3-5) of the WT. Values represent means ± SD. Letters indicate significant differences of genotype × tissue interactions for each gene (two-way ANOVA with post hoc LSD test; $n = 4$; $P < 0.001$). a.u., arbitrary unit.

SUR1, and *UGT74C1* by qRT-PCR. Gene expression was lowest in young leaves and gradually increased with leaf age. Although tissue-specific biosynthetic rates cannot be rigorously determined by expression analysis of biosynthetic genes, these findings suggest that glucosinolates are primarily produced in old leaves and subsequently transported to young ones (Fig. 1*C*). To test this hypothesis, we analyzed the tissue-specific glucosinolate distribution in knockout mutants of genes encoding the well-characterized H^+/glucosinolate symporters NPF2.10/GTR1, NPF2.11/GTR2, and NPF2.9/GTR3 (21, 22). In *gtr1 gtr2* double knockout mutants, the gradient of total glucosinolates across leaf groups was abolished, demonstrating that GTR1/GTR2-mediated transport establishes the ontogenetic glucosinolate distribution in the rosette (Fig. 1*B*). Compared to WT, total glucosinolate levels were significantly reduced in young leaves and increased in old and mature ones, indicating that GTR1 and GTR2 are responsible for the export of glucosinolates from old leaves. Intriguingly, indolic glucosinolates—particularly 1-methoxy-indol-3-ylmethyl glucosinolate—retained a gradual distribution in *gtr1 gtr2* (*SI Appendix*, Fig. S1). Analysis of the tissue-specific glucosinolate distribution in *gtr1 gtr2 gtr3* triple knockout mutants—GTR3 has high affinity toward indolic glucosinolates—showed that high indolic glucosinolate levels in young leaves are still maintained in the absence of all three glucosinolate transporters, despite significant accumulation in old and mature leaves leading to their uniform distribution among leaf cohorts (*SI Appendix*, Fig. S1). To test whether absence of a glucosinolate supply from old and mature leaves affects tissue-specific expression of biosynthetic genes, we analyzed the spatial gene expression of key biosynthetic enzymes in *gtr1 gtr2* and found significant genotype × tissue interactions for *CYP79B2*, *CYP83A1*, *MAM3*, and *SUR1* (Fig. 1*C*). The transcript levels of these genes were reduced in old leaves, indicating that *GTR1*/*GTR2*-dependent overaccumulation of glucosinolates in old leaves may lead to feedback inhibition of glucosinolate biosynthesis gene expression (Fig. 1 *B* and *C*). This supports the idea that the altered glucosinolate distribution in *gtr1 gtr2* is caused by perturbation of transport that cannot be entirely compensated for by inducing the expression of biosynthetic genes in young leaves.

Next, we leveraged the uniform distribution of glucosinolates in the rosette of *gtr1 gtr2* mutants and used glucosinolate-based chemical defense as a model to explore the effect of defense distribution on herbivore feeding preference. We performed a bioassay using larvae of *Spodoptera littoralis*, a generalist insect herbivore that infests plants from at least 40 families, including the families of the Brassicales order and many economically important species (23). *S. littoralis* showed a strong preference (100%, $n = 90$) for feeding on old and mature leaves of the WT, as *S. littoralis* larvae caused severe feeding damage on old and mature leaves while avoiding the young ones (Fig. 2 *A* and *B* and *SI Appendix*, Fig. S2). This feeding preference inversely correlates with leaf glucosinolate concentrations and is consistent with the predictions of the optimal defense theory for defense

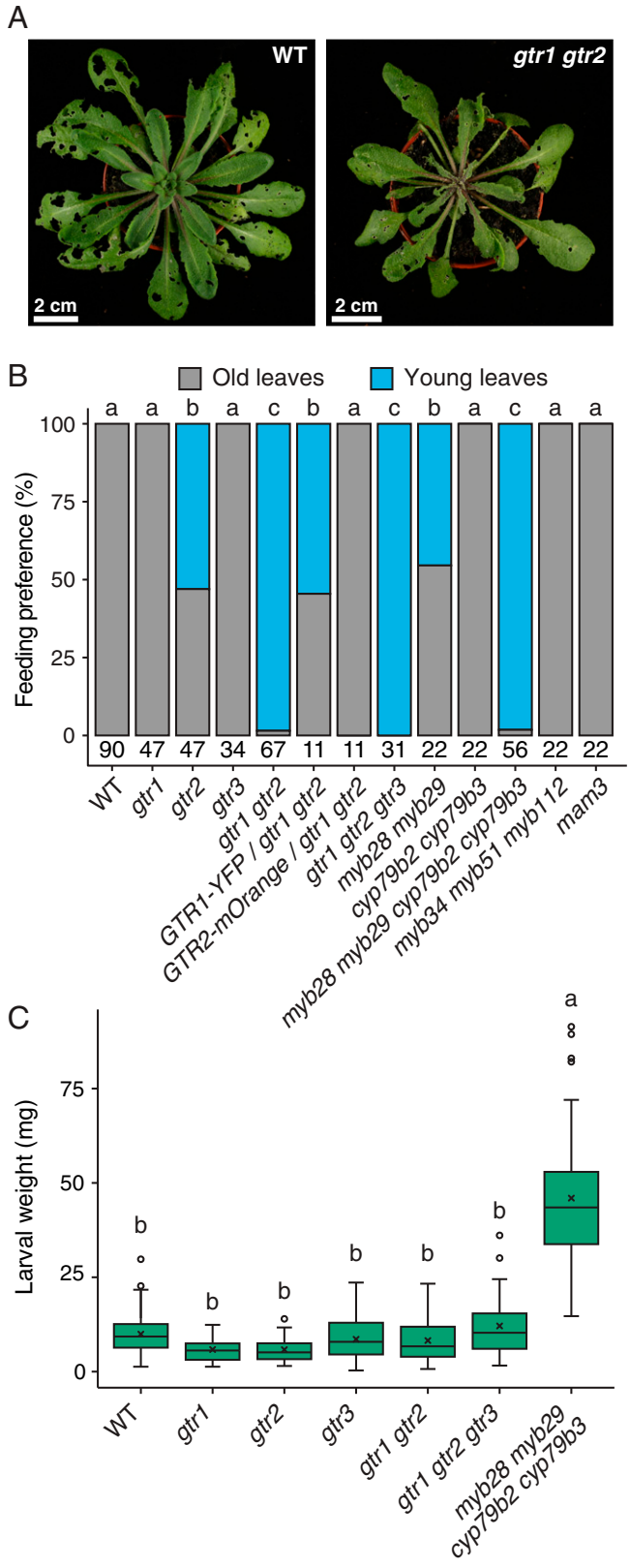

Fig. 2. *GTR1* and *GTR2* transporters determine the feeding preference of larvae of generalist herbivore *S. littoralis*. (*A*) Photographs of 5-wk-old WT and *gtr1gtr2* double knockout mutant plants imaged 8 d after infection with newly hatched larvae in a nonchoice experimental set-up. Note that the young leaves in the center of the rosette are almost completely consumed in *gtr1 gtr2*. (Scale bar, 2 cm.) (*B*) Quantification of *S. littoralis*–feeding pattern on WT, glucosinolate transporter mutants (*gtr1*, *gtr2*, *gtr3*, *gtr1 gtr2*, *gtr1 gtr2 gtr3*, *GTR1-YFP/gtr1 gtr2*, and *GTR2-mOrange/gtr1 gtr2*) and glucosinolate biosynthesis mutants (*myb28 myb29*, *cyp79b2 cyp79b3*, *myb28 myb29 cyp79b2 cyp79b3*, *myb34 myb51 myb112*, and *mam3*). Number of biological replicates (*n*) is indicated below the stacked bars. Pooled data from one to eight independent replicates are shown. Letters above stacked bars indicate significant differences between genotypes (Fisher's exact test, $P < 0.05$). (*C*) Quantification of larval weight of *S. littoralis* following 8 d of feeding on 4-wk-old WT and mutant plants. Letters depict significant differences between genotypes (two-way ANOVA with post hoc Tukey's HSD test; $n = 103; 30; 33; 38; 83; 36; 44$; $P < 0.001$). Pooled data from three independent replicates are shown. "x" indicates mean.

distribution within the plant. Strikingly, we found that the feeding preference is inverted (98.5%, $n = 67$) on *gtr1 gtr2* (Fig. 2 *A* and *B*). Thus, the spatial pattern of glucosinolate distribution governs the feeding preference of *S. littoralis*. This conclusion is further supported by the observation of a preference for young leaves (100%, $n = 56$) on glucosinolate-deficient *myb28 myb29 cyp79b2 cyp79b3* quadruple mutants (Fig. 2*B* and *SI Appendix*, Fig. S3). As *GTR1* and *GTR2* expression is not affected in the quadruple mutant (24), the finding demonstrates that the feeding preference specifically depends on glucosinolates, thus eliminating a potential role of GTR1/GTR2-mediated distribution of other metabolites (e.g., nutrients or hormones). Overaccumulation of glucosinolates in old leaves of *gtr1 gtr2* cannot explain the feeding preference, as larvae also avoided feeding on old leaves of glucosinolate-deficient plants, probably due to the relative nutritional value and digestibility (Figs. 1*B* and 2*B*). The feeding preference for young leaves on biosynthetic and transport-deficient mutants supports the idea that high glucosinolate concentrations in young leaves are crucial to their protection. Consistent with previous studies showing that glucosinolates delay larval development of *S. littoralis* because of energy-consumptive detoxification (25), larvae gained significantly more weight on glucosinolate-deficient plants compared to WT (Fig. 2*C*). By contrast, *S. littoralis* feeding on glucosinolate transporter mutants did not affect the weight of larvae (Fig. 2*C*), possibly because the ingestion of the residual glucosinolates in young leaves of *gtr1 gtr2* is sufficient to delay growth compared to the glucosinolate-free young leaves of the quadruple mutant. Hence, herbivore performance in terms of larval weight gain is not affected by shifting herbivore feeding to young leaves. We set out to assess plant fitness by quantifying fecundity, even though it already seems reasonable to infer that fitness cost will be incurred for plants that have lost most of their young leaves. However, when we exposed plants to larvae long term, *gtr1 gtr2*, *gtr1 gtr2 gtr3*, and *myb28 myb29 cyp79b2 cyp79b3* mutants were not surviving to fruiting. We observed an overall survival rate of 0% ($n = 11$) for *gtr1 gtr2*, *gtr1 gtr2 gtr3*, and *myb28 myb29 cyp79b2 cyp79b3* mutant plants, while WT plants survived to bolting (100%, $n = 11$) in two experimental replicates. In conclusion, *A. thaliana* profits from transporter-mediated, nonuniform glucosinolate distribution in the rosette, which prevents herbivore attacks against the most valuable and vulnerable tissues, thus providing physiological evidence for the central hypothesis of the optimal defense theory.

In addition to defense allocation within the plant, the optimal defense theory also predicts that defense is increased upon attack. To test how the tissue-specific distribution of glucosinolates is affected by the plant–herbivore interaction, we measured their concentration in young WT leaves upon *S. littoralis* feeding. As young leaves of the mutants were completely consumed during bioassays, we further used mechanical wounding to mimic generalist herbivores. Indolic glucosinolate levels were significantly (approximately threefold) induced by both treatments, indicating that herbivore-associated molecular patterns are negligible for this

PLANT BIOLOGY

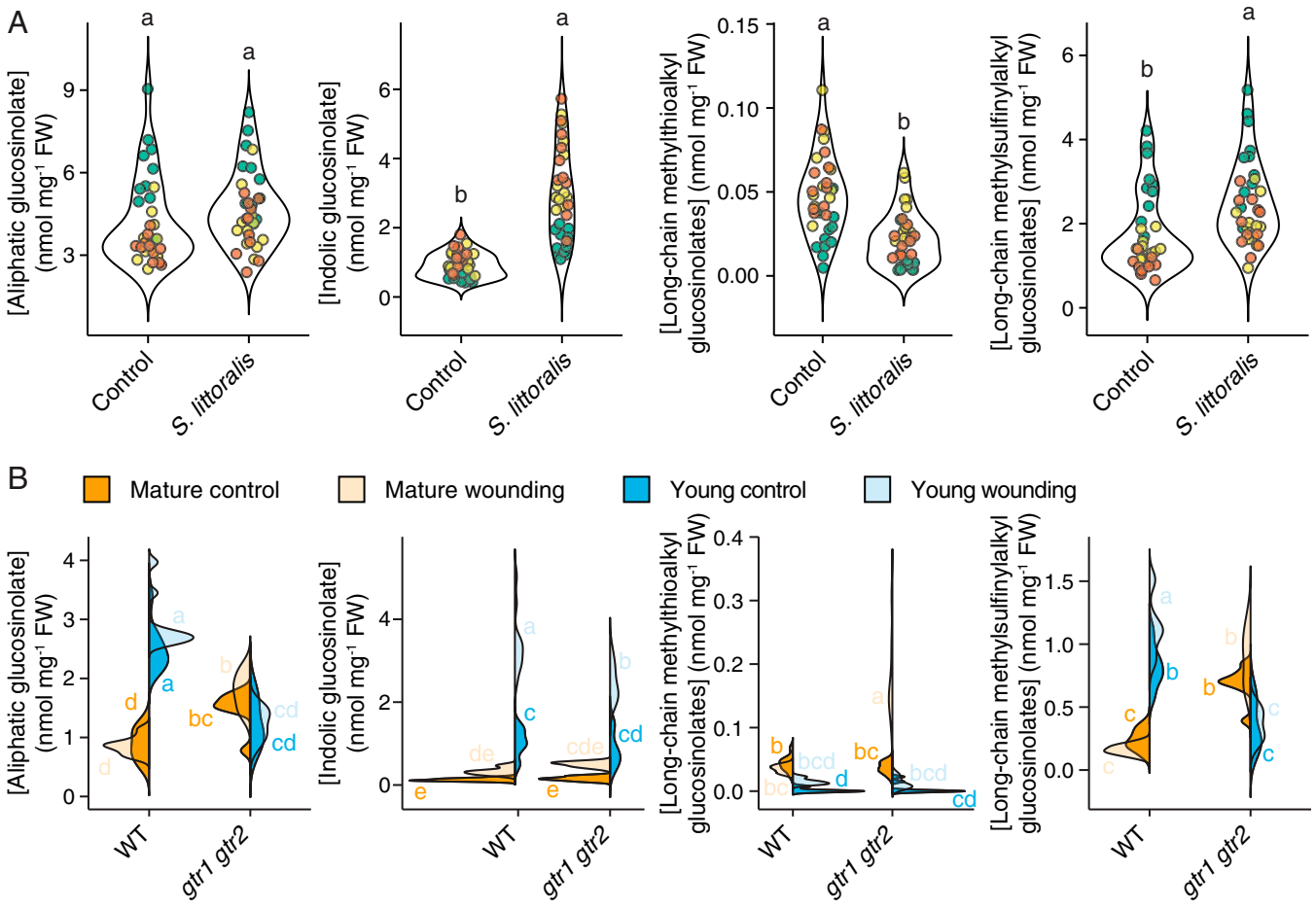

Fig. 3. Tissue-specific accumulation of glucosinolates upon mechanical wounding and herbivore attack. (*A*) Perturbations of aliphatic, indolic, long-chain methylthioalkyl, and long-chain methylsulfinylalkyl glucosinolate concentrations in young leaves (L9+) of WT plants following 8 d of *S. littoralis* feeding. Letters depict significant differences among treatments (two-way ANOVA with post hoc Tukey's HSD test; $n = 11$; $P < 0.001$). Pooled data from three independent replicates are shown. Data points represent biological replicates and are color coded according to experimental replicates. (*B*) Tissue-specific perturbations of aliphatic, indolic, long-chain methylthioalkyl, and long-chain methylsulfinylalkyl glucosinolate concentrations in mature (L6-8; orange) and young (L9+; blue) leaves of WT and *gtr1 gtr2* double knockout mutants upon repetitive mechanical wounding of old leaves (L3-5). Letters indicate significant differences of genotype × tissue interactions (two-way ANOVA with post hoc Tukey's HSD test, $n = 10$, $P < 0.001$). Leaves were grouped according to Fig. 1*A*. FW, fresh weight.

response (Fig. 3). These increases also occurred in *gtr1 gtr2* and *gtr1 gtr2 gtr3*, suggesting tissue-specific induction of de novo indolic glucosinolate biosynthesis upon wounding (Fig. 3*B* and *SI Appendix*, Fig. S5), which is consistent with the reported up-regulation of genes involved in indolic glucosinolate biosynthesis upon *S. littoralis* feeding and wounding (26). Furthermore, *S. littoralis* exhibited a feeding preference for young leaves on aliphatic glucosinolate-deficient *myb28 myb29*, and not indolic glucosinolate-deficient *cyp79b2 cyp79b3* and *myb34 myb51 myb122* mutants, demonstrating that aliphatic, but not indolic glucosinolates, are critical for establishing the feeding preference (Fig. 2*B* and *SI Appendix*, Fig. S3). Indeed, the levels of long-chain aliphatic glucosinolates in young leaves increased significantly upon both feeding and wounding (*SI Appendix*, Figs. S4 and S5). Moreover, specifically long-chain methylsulfinylalkyl glucosinolates accumulate, indicating that feeding-inflicted wounding triggers *S*-oxygenation on the side chain in young leaves (Fig. 3 and *SI Appendix*, Figs. S4 and S5). *S*-oxygenation in response to wounding was attenuated in *gtr1 gtr2* and, interestingly, the mutant overaccumulated the corresponding precursors (i.e., methylthioalkyl glucosinolates) in unwounded mature leaves (Fig. 3*B* and *SI Appendix*, Fig. S5). Yet the accumulation and modification of long-chain aliphatic glucosinolates is not required for the defense of young leaves, as *S. littoralis* showed a feeding preference for old leaves on long-chain aliphatic glucosinolate-deficient *mam3* mutants (Fig. 2*B* and *SI Appendix*, Fig. S3). Hence, basal levels of total aliphatic glucosinolates are critical for optimal defense of young tissues against generalist herbivores such as *S. littoralis*.

Based on our results, we propose a model that predicts a function for mature tissues in serving as relays that orchestrate glucosinolate biosynthesis and transport to protect tissues with higher fitness values from attack (*SI Appendix*, Fig. S6). Briefly, glucosinolates are translocated from root to shoot via the xylem, which is controlled by a GTR1/GTR2/GTR3-mediated retention mechanism that is inactivated upon feeding-induced wounding. This is supported by our finding that mature leaves of untreated *gtr1 gtr2 gtr3* mutants display elevated long-chain methylthioalkyl glucosinolate concentrations, which could not be further induced by wounding (*SI Appendix*, Fig. S5). In mature leaves, glucosinolates are GTR1/GTR2-dependently loaded into the phloem for transport to young leaves, which is supported by the expression of *GTR1* and *GTR2* in the vasculature and hydathodes (*SI Appendix*, Fig. S7). Young,

immature plant tissues are well known to be strong sinks for carbon and nitrogen that are supplied by mature tissues. Because of metabolic constraints, biosynthesis of specialized metabolites—such as glucosinolates—in mature leaves may thus be more adaptive for plants than producing them in young leaves, which is consistent with the subhypothesis of the optimal defense theory predicting a trade-off between defense and other plant functions such as growth and reproduction. Higher defensive investment in young tissue is not limited to glucosinolates in Brassicales. Direct defenses, such as alkaloids, phenolic compounds, iridoid glycosides, cyanogenic glycosides, and furanocoumarins, were also shown to be higher in young leaves than old ones (8). Similar within-plant distributions were also found for indirect defenses (e.g., volatile organic compounds) and defensive structures (e.g., trichomes) (8). Most of the nonuniformly distributed direct and indirect defenses are subject to transport, as they can be detected in phloem and/or xylem exudates (27). For example, pyrrolizidine alkaloids act as a defense against generalist herbivores and are transported from old to young leaves of *Cynoglossum officinale* (28). Benzylisoquinoline alkaloids (e.g., morphine in *Papaver somniferum*) are (at least partly) synthesized in sieve elements of the phloem and stored in laticifers (29). In tobacco, nicotine is synthesized in the root and transported to the leaves via the xylem in response to herbivore feeding (30, 31). In recent years, numerous transporters with affinities toward defensive metabolites have been identified (32). Based on the current knowledge, it is conceivable that transporters are important for the distribution of other types of chemical defenses in other species (33). As the relative value and vulnerability of plant tissues change during development, defenses need to be tightly regulated to reduce metabolic costs. Metabolic costs for defense transport are largely unknown, but it seems likely that total costs are reduced if defenses are (re)allocated to the target tissues. To sum up, using glucosinolate-based defense of *A. thaliana* against the generalist herbivore *S. littoralis*, we were able to provide experimental evidence for the physiological aspects of the optimal defense theory and highlight the importance of coordinating biosynthesis and transport processes of defensive metabolites to obtain the most favorable distribution within a plant for optimizing growth and defense.

Methods

Biological Material. *A. thaliana* (L.) Heynhold plants were grown on soil in a walk-in climate chamber under short-day conditions (10 h light, 150 μmol · m^{-2} · s^{-1}, 21 °C, 70% humidity). The Columbia-0 accession was used as WT. The following, previously described transfer DNA insertion and transgenic lines were used: *myb28 myb29* (34), *cyp79b2 cyp79b3* (35), *myb28 myb29 cyp79b2 cyp79b3* (24), *myb34 myb51 myb122* (36), *mam3* (37), *gtr1* (21), *gtr2* (21), *gtr3* (22), *gtr1 gtr2* (21), *gtr1 gtr2 gtr3* (22), *pGTR1::NLS-GUS-GFP* (21), *pGTR2::GTR2-NLS-GUS-GFP* (21), *pGTR1::GTR1-YFP* in *gtr1 gtr2* (21), and *pGTR2::GTR2-mOrange2* in *gtr1 gtr2* (21). Egg clutches of *S. littoralis* Boisduval (African cotton leafworm) were a generous gift from Daniel G. Vassão of the Max Planck Institute for Chemical Ecology were and reared on an artificial diet based on white beans at 18 to 20 °C under natural light (25, 38).

Desulfoglucosinolate Analysis by LC-MS. Leaves of 4-wk-old plants were harvested according to the harvesting scheme presented in Fig. 1*A* and immediately submerged in 85% methanol containing 50 μM *p*-hydroxybenzyl glucosinolate as internal standard. Desulfoglucosinolates were purified as described previously (39). Analysis was performed on an Advance ultra-high performance liquid chromatography system (Bruker) coupled to an EVOQ Elite TripleQuad mass spectrometer (Bruker) equipped with an electrospray ion source operated in positive ionization mode, as previously described (40). Detailed values for mass transitions have been described previously (41, 42). Linearity in ionization efficiencies were verified by analyzing dilution series. Glucosinolate concentrations were normalized to fresh weight. Glucosinolates were grouped as follows: aliphatic (3-methylthiopropyl, 3-methylsulfinylpropyl, 4methylthiobutyl, 4-methylsul finylbutyl, 5-methylsulfinylpentyl, 7-methylthioheptyl, 7-methylsulfinylheptyl, 8-methylthiooctyl, and 8-methylsulfinyloctyl glucosinolate), indolic (indol-3-ylmethyl, 1-methoxy-indol-3-ylmethyl, and 4-methoxy-indol-3-ylmethyl glucosinolate), short-chain aliphatic (3-methylthiopropyl, 3-methylsulfinylpropyl, 4methylthiobutyl, 4-methylsulfinylbutyl, and 5-methylsulfinylpentyl glucosinolate), long-chain aliphatic (7-methylthioheptyl, 7-methylsulfinylheptyl, 8-methylthiooctyl, and 8-methylsulfinyloctyl glucosinolate), methylthioalkyl (3-methylthiopropyl, 4methylthiobutyl, 7-methylthioheptyl, and 8-methyl thiooctyl glucosinolate), and methylsulfinylalkyl (3-methylsulfinylpropyl, 4-methylsulfinylbutyl, 5-methylsulfinylpentyl, 7-methylsulfinylheptyl, and 8-methylsulfinyloctyl glucosinolate) glucosinolates.

β-Glucuronidase Activity (GUS) Staining. Plant material was collected in 90% acetone, incubated for at least 20 min, and washed with 50 mM sodium phosphate buffer pH 7.0 for 5 to 10 min. The rinsing solution was replaced with staining mix [50 mM sodium phosphate buffer pH 7.0, 0.1% Triton X-100, 0.5 mM $K_4Fe(CN)_6$, 0.5 mM $K_3Fe(CN)_6$, and 0.5 mg/mL X-Gluc]. Plant material was then vacuum infiltrated for 5 min at room temperature and incubated at 37 °C in the dark overnight. The reaction was stopped by replacing the staining solution with 70% ethanol, which was exchanged several times until the tissue was completely cleared. Images were taken using a Leica M205 FA stereomicroscope (Leica Microsystems) or an Epson Perfection V550 Photo color scanner (Seiko Epson Corporation). White balance was adjusted using Photoshop CC (version 19.0, Adobe Systems Inc.).

Insect Bioassays. Neonate *S. littoralis* were placed on 3.5- to 4-wk-old plants. Plant genotypes were contained in separate plastic boxes. In each box, 11 plants were distributed, and three larvae were placed at the center of the rosette of each individual plant. Larvae were able to move between plants within each box and allowed to feed for 7 to 8 d. The mass of individual larvae was determined by a Mettler Toledo PG503-S DeltaRange precision balance (Mettler Toledo).

RNA Extraction, cDNA Synthesis, and RT-qPCR. For total RNA extraction, designated plant material of three plants was combined into one biological replicate and snap frozen in liquid nitrogen followed by homogenization to fine powder in a RETSCH bead mill. RNA was extracted using the Sigma Spectrum Plant Total RNA kit. Electrophoresis was used to assess native RNA quality on a 1% agarose gel. Next, 1 μg total RNA was DNase1 treated (Sigma) and used for cDNA synthesis (iScript from Bio-Rad) with a blend of random hexamer and oligo(dT) primers in a 20-μL reaction. The obtained cDNA was 1:10 diluted in water, and 2 μL were used in a 10-μL SYBR green (PowerUp SYBR, Applied Biosystems) RT-qPCR reaction, run in a CFX384 Touch real-time PCR detection system from Bio-Rad. RT-qPCR of genes of interest and the housekeeping transcript *UBC21* (At5g25760) were performed in standard cycling mode condition according to the SYBR green manufacturer. Three technical replicates were run for each biological replicate. Relative expression was calculated with kinetic PCR efficiency correction and normalized to *UBC21* and further to the WT sample "Old leaves (L3-5)." Oligonucleotide sequences used in this study can be found in *SI Appendix*, Table S1.

Mechanical Wounding. Wounds were inflicted with forceps parallel to the longitudinal axis of the third, fourth, and fifth leaves. The first wound was made at the leaf tip, the second wound was made so that it abutted the first, and so on, until 40 to 50% of the leaf was wounded. The wounding was repeated three times in 3-h intervals. Unwounded plants served as a control and were randomly distributed among wounded plants. The plant material was harvested 24 h after the first round of wounding.

Data Visualization and Statistics. Data visualization and statistical analyses were performed in R (43). Plots were produced using the ggplot2 package (44). Boxplots show median (center line), mean (cross), first quartile (lower hinge), third quartile (upper hinge), whiskers (extending 1.5 times the interquartile range), and possible outliers (circles). ANOVA analyses and post hoc Tukey's Honestly Significant Difference (HSD) or Least Significant Difference (LSD) tests were performed using the agricolae and nmle packages (45, 46). Prior to analysis, data were checked for normality and scedasticity using diagnostic plots. Glucosinolate concentrations were fitted to a linear model as a function of genotype × tissue × experimental replicate (Fig. 1*B* and *SI Appendix*, Fig. S1), treatment × experimental replicate (Fig. 3*A* and *SI Appendix*, Fig. S4), or genotype × treatment × tissue (Fig. 3*B* and *SI Appendix*, Fig. S5). Relative transcript levels were fitted to a linear model as a function of genotype × tissue (Fig. 1*C*). Larval weight was fitted to a linear model as a function of genotype × experimental replicate (Fig. 2*C* and *SI Appendix*, Figs. S2*B* and S3*B*). Additionally, glucosinolate concentrations were fitted to a mixed-effects model accounting for box effects as a random factor (Fig. 3*A*). A likelihood ratio test was employed to compare linear and mixed-effects models and revealed nonsignificant *P* values for each independent variable. Based

on this result, linear models were preferred over mixed-effects models. Fisher's exact test was performed using a Monte Carlo simulation with 10^7 replicates. Post hoc pairwise comparison with Bonferroni-adjusted *P* values was performed using the rcompanion package (47). *F* values, *P* values, and degrees of freedom can be found in *SI Appendix*, Tables S2 and S3.

Data Availability. All study data are included in the article and/or *SI Appendix*.

ACKNOWLEDGMENTS. We thank D. G. Vassão and V. Jeschke for providing *S. littoralis* eggs. This work was funded by the Danish National Research Foundation (Grant DNRF99).

1. D. McKey, "The distribution of secondary compounds within plants" in *Herbivores: Their Interaction with Secondary Plant Metabolites*, G. A. Rosenthal, D. H. Janzen, Eds. (Academic Press, 1979), pp. 55–134.
2. D. McKey, Adaptive patterns in alkaloid physiology. *Am. Nat.* **108**, 305–320 (1974).
3. D. F. Rhoades, "Evolution of plant chemical defense against herbivores" in *Herbivores: Their Interaction with Secondary Plant Metabolites*, G. A. Rosenthal, D. H. Janzen, Eds. (Academic Press, 1979), pp. 3–54.
4. N. Stamp, Out of the quagmire of plant defense hypotheses. *Q. Rev. Biol.* **78**, 23–55 (2003).
5. D. Li, R. Halitschke, I. T. Baldwin, E. Gaquerel, Information theory tests critical predictions of plant defense theory for specialized metabolism. *Sci. Adv.* **6**, eaaz0381 (2020).
6. A. R. Zangerl, C. E. Rutledge, The probability of attack and patterns of constitutive and induced defense: A test of optimal defense theory. *Am. Nat.* **147**, 599–608 (1996).
7. R. Shroff, F. Vergara, A. Muck, A. Svatos, J. Gershenzon, Nonuniform distribution of glucosinolates in *Arabidopsis thaliana* leaves has important consequences for plant defense. *Proc. Natl. Acad. Sci. U.S.A.* **105**, 6196–6201 (2008).
8. S. Meldau, M. Erb, I. T. Baldwin, Defence on demand: Mechanisms behind optimal defence patterns. *Ann. Bot.* **110**, 1503–1514 (2012).
9. F. Schweizer *et al.*, *Arabidopsis* basic helix-loop-helix transcription factors MYC2, MYC3, and MYC4 regulate glucosinolate biosynthesis, insect performance, and feeding behavior. *Plant Cell* **25**, 3117–3132 (2013).
10. R. J. Hopkins, N. M. van Dam, J. J. A. van Loon, Role of glucosinolates in insect-plant relationships and multitrophic interactions. *Annu. Rev. Entomol.* **54**, 57–83 (2009).
11. I. Winde, U. Wittstock, Insect herbivore counteradaptations to the plant glucosinolate-myrosinase system. *Phytochemistry* **72**, 1566–1575 (2011).
12. M. Bekaert, P. P. Edger, C. M. Hudson, J. C. Pires, G. C. Conant, Metabolic and evolutionary costs of herbivory defense: Systems biology of glucosinolate synthesis. *New Phytol.* **196**, 596–605 (2012).
13. P. P. Edger *et al.*, The butterfly plant arms-race escalated by gene and genome duplications. *Proc. Natl. Acad. Sci. U.S.A.* **112**, 8362–8366 (2015).
14. E. K. Barto, D. Cipollini, Testing the optimal defense theory and the growth-differentiation balance hypothesis in *Arabidopsis thaliana*. *Oecologia* **146**, 169–178 (2005).
15. P. D. Brown, J. G. Tokuhisa, M. Reichelt, J. Gershenzon, Variation of glucosinolate accumulation among different organs and developmental stages of *Arabidopsis thaliana*. *Phytochemistry* **62**, 471–481 (2003).
16. M. M. Blake-Kalff, K. R. Harrison, M. J. Hawkesford, F. J. Zhao, S. P. McGrath, Distribution of sulfur within oilseed rape leaves in response to sulfur deficiency during vegetative growth. *Plant Physiol.* **118**, 1337–1344 (1998).
17. H.-H. Cao, Z.-F. Zhang, X.-F. Wang, T.-X. Liu, Nutrition versus defense: Why *Myzus persicae* (green peach aphid) prefers and performs better on young leaves of cabbage. *PLoS One* **13**, e0196219 (2018).
18. R. J. Hopkins, B. Ekbom, L. Henkow, Glucosinolate content and susceptibility for insect attack of three populations of *Sinapis alba*. *J. Chem. Ecol.* **24**, 1203–1216 (1998).
19. A. L. Shelton, Within-plant variation in glucosinolate concentrations of *Raphanus sativus* across multiple scales. *J. Chem. Ecol.* **31**, 1711–1732 (2005).
20. F. R. Badenes-Perez, J. Gershenzon, D. G. Heckel, Insect attraction versus plant defense: Young leaves high in glucosinolates stimulate oviposition by a specialist herbivore despite poor larval survival due to high saponin content. *PLoS One* **9**, e95766 (2014).
21. H. H. Nour-Eldin *et al.*, NRT/PTR transporters are essential for translocation of glucosinolate defence compounds to seeds. *Nature* **488**, 531–534 (2012).
22. M. E. Jørgensen *et al.*, Origin and evolution of transporter substrate specificity within the NPF family. *eLife* **6**, e19466 (2017).
23. H. S. Salama, N. Z. Dimetry, S. A. Salem, On the host preference and biology of the cotton leaf worm *Spodoptera littoralis*. *Z. Angew. Entomol.* **67**, 261–266 (1970).
24. R. Müller *et al.*, Differential effects of indole and aliphatic glucosinolates on lepidopteran herbivores. *J. Chem. Ecol.* **36**, 905–913 (2010).
25. V. Jeschke *et al.*, How glucosinolates affect generalist lepidopteran larvae: Growth, development and glucosinolate metabolism. *Front Plant Sci* **8**, 1995 (2017).
26. P. Reymond *et al.*, A conserved transcript pattern in response to a specialist and a generalist herbivore. *Plant Cell* **16**, 3132–3147 (2004).
27. J. C. Schultz, H. M. Appel, A. P. Ferrieri, T. M. Arnold, Flexible resource allocation during plant defense responses. *Front Plant Sci* **4**, 324 (2013).
28. N. M. V. Dam, T. J. D. Jong, Y. Iwasa, T. Kubo, Optimal distribution of defences: Are plants smart investors? *Funct. Ecol.* **10**, 128–136 (1996).
29. A. Singh, I. M. Menéndez-Perdomo, P. J. Facchini, Benzylisoquinoline alkaloid biosynthesis in opium poppy: An update. *Phytochem. Rev.* **18**, 1457–1482 (2019).
30. T. E. Ohnmeiss, I. T. Baldwin, Optimal defense theory predicts the ontogeny of an induced nicotine defense. *Ecology* **81**, 1765–1783 (2000).
31. I. T. Baldwin, M. J. Karb, T. E. Ohnmeiss, Allocation of 15N from nitrate to nicotine: Production and turnover of a damage-induced mobile defense. *Ecology* **75**, 1703–1713 (1994).
32. U. Gani, R. A. Vishwakarma, P. Misra, Membrane transporters: The key drivers of transport of secondary metabolites in plants. *Plant Cell Rep.* **40**, 1–18 (2021).
33. M. Erb, P. Reymond, Molecular interactions between plants and insect herbivores. *Annu. Rev. Plant Biol.* **70**, 527–557 (2019).
34. J. Beekwilder *et al.*, The impact of the absence of aliphatic glucosinolates on insect herbivory in Arabidopsis. *PLoS One* **3**, e2068 (2008).
35. Y. Zhao *et al.*, Trp-dependent auxin biosynthesis in *Arabidopsis*: Involvement of cytochrome P450s CYP79B2 and CYP79B3. *Genes Dev.* **16**, 3100–3112 (2002).
36. H. Frerigmann, T. Gigolashvili, MYB34, MYB51, and MYB122 distinctly regulate indolic glucosinolate biosynthesis in *Arabidopsis thaliana*. *Mol. Plant* **7**, 814–828 (2014).
37. S. Textor, J.-W. de Kraker, B. Hause, J. Gershenzon, J. G. Tokuhisa, MAM3 catalyzes the formation of all aliphatic glucosinolate chain lengths in *Arabidopsis*. *Plant Physiol.* **144**, 60–71 (2007).
38. V. Jeschke, J. Gershenzon, D. G. Vassão, "Chapter eight - insect detoxification of glucosinolates and their hydrolysis products" in *Advances in Botanical Research*, S. Kopriva, Ed. (Academic Press, 2016), vol. 80, pp. 199–245.
39. T. G. Andersen *et al.*, Integration of biosynthesis and long-distance transport establish organ-specific glucosinolate profiles in vegetative *Arabidopsis*. *Plant Cell* **25**, 3133–3145 (2013).
40. D. Xu *et al.*, GTR-mediated radial import directs accumulation of defensive glucosinolates to sulfur-rich cells in the phloem cap of *Arabidopsis* inflorescence stem. *Mol. Plant* **12**, 1474–1484 (2019).
41. L. M. Jensen, H. S. K. Jepsen, B. A. Halkier, D. J. Kliebenstein, M. Burow, Natural variation in cross-talk between glucosinolates and onset of flowering in *Arabidopsis*. *Front Plant Sci* **6**, 697 (2015).
42. C. Crocoll, B. A. Halkier, M. Burow, Analysis and quantification of glucosinolates. *Curr. Protoc. Plant Biol.* **1**, 385–409 (2016).
43. R Core Team, *R: A Language and Environment for Statistical Computing* (R Foundation for Statistical Computing, 2019).
44. H. Wickham, *ggplot2 - Elegant Graphics for Data Analysis*, (Springer International Publishing, ed. 2, 2016).
45. F. de Mendiburu, agricolae: Statistical Procedures for Agricultural Research. (R package version 1.3-5, 2020). https://CRAN.R-project.org/package=agricolae. Accessed 1 January 2021.
46. J. Pinheiro, D. Bates, S. DebRoy, D. Sarkar, R Core Team, nlme: Linear and Nonlinear Mixed Effects Models. (R package version 3.1–148, 2020). https://CRAN.R-project.org/package=nlme. Accessed 1 January 2021.
47. S. Mangiafico, rcompanion: Functions to Support Extension Education Program Evaluation. (R package version 2.3. 26, 2020). https://CRAN.R-project.org/package=rcompanion. Accesssed 1 January 2021.